Supplementary Information (SI) for Journal of Materials Chemistry A.

Supplementary Information

Optimized MnO_2 photocathode by doping engineering for high capacity and stability photo-assisted zinc-ion batteries

Dongyue Tian#, Xinyu Gao#, Jiayu Wang, Ruyu Sun, Jiaming Liu, Jingjing Cao* and Wei Feng*

College of Chemistry, Chemical Engineering and Resource Utilization, Northeast Forestry University, Harbin 150040, China

*Corresponding author. E-mail: caojingjingcjj@163.com; wfeng@nefu.edu.cn

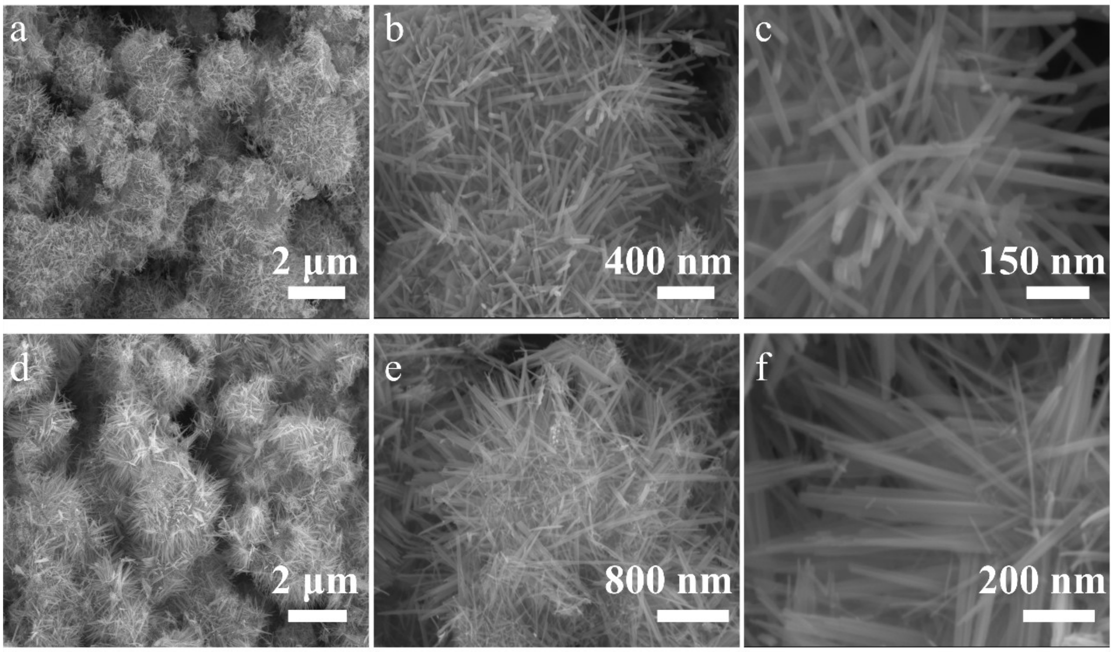

Fig. S1 (a-c) SEM images of Al-MnO_2. (d-f) SEM images of MnO_2.

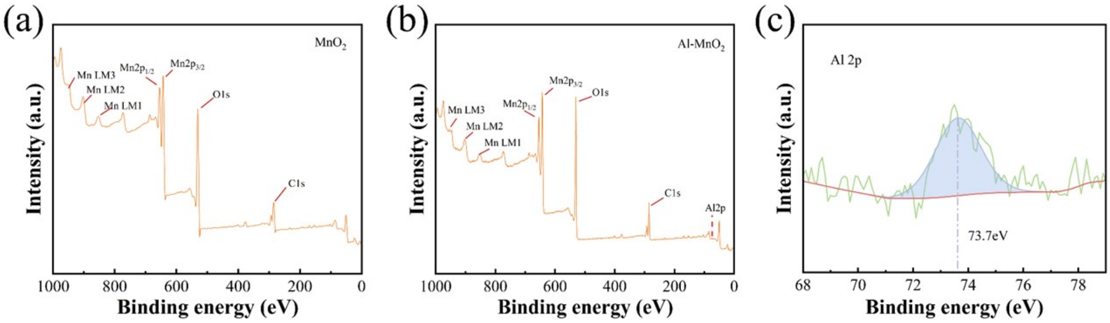

Fig. S2 (a) Full XPS spectra of MnO_2. (b) Full XPS spectra of Al-MnO_2. (c) The high-resolution Al 2p XPS spectra.

Table S1. The Mn^{3+}/Mn^{4+} integrated peak area of MnO_2 and Al-MnO_2.

	Mn^{3+}	Mn^{4+}	Mn^{3+}/Mn^{4+}
MnO_2	443757.26	134047.13	3.31
Al-MnO_2	476621.00	114607.95	4.16

Table S2. The ratios correspond to different oxygen species of MnO_2 and Al-MnO_2.

	Absorbed O	Defective O	Lattice O
MnO_2	26.8%	12.7%	60.5%
Al-MnO_2	11.7%	29.2%	59.1%

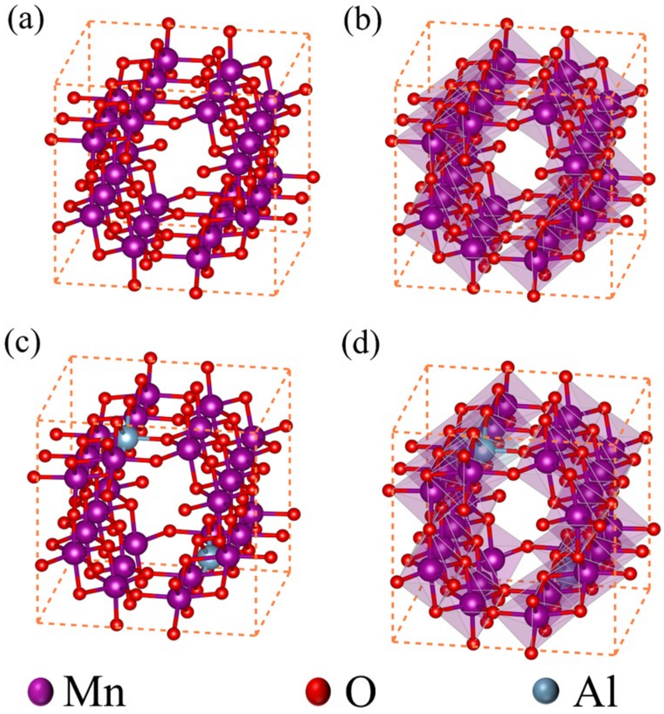

Fig. S3 (a) and (b) Model structure for MnO_2. (c) and (d) Model structure for Al-MnO_2.

The methodology of theoretical simulation: All the spin-unrestricted density functional theory with on-site Coulomb repulsion term U (DFT+U) calculations were performed using Vienna Ab-initio Simulation Package (VASP). The exchange and correlation potential were determined with the Perdew, Burke, and Ernzerhof within the generalized gradient approximation (PBE-GGA) functional. The interaction between electrons and ions were described by using projector augmented wave (PAW) method. A thermal smearing of 0.05 eV to the orbital occupation was applied to speed up electronic convergence. The Brillouin zone sampling was performed on meshes with a k-point spacing of 0.04 $Å^{-1}$. The convergence tolerance of electronic structure and geometry optimization was 1×10^{-5} eV, 0.02 eV/Å, respectively. The plane wave cut-off was set to 400 eV. In the DFT + U method, we picked up the effective U values of 4.0 eV to treat the localized nature of Mn 3d electrons, which can describe the on-site Coulomb and exchange interaction of localized electrons. In the Al-MnO_2 model, two Mn atoms (8.33 %) were replaced with Al, and one O atom (2.1 %) was removed to consider the defect.

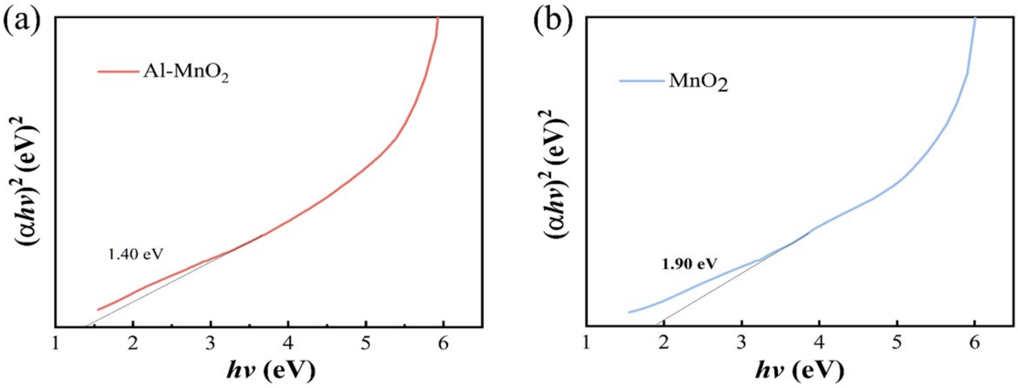

Fig. S4 The Tauc plots of (a) Al-MnO_2 and (b) MnO_2.

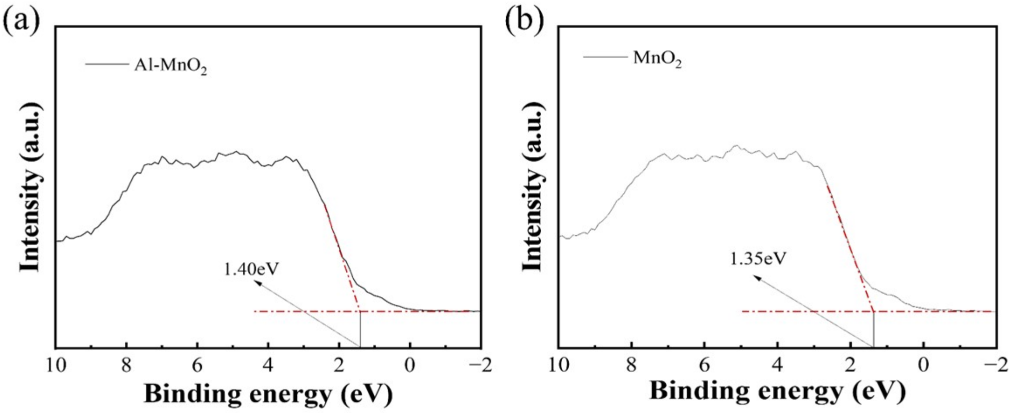

Fig. S5 XPS-VB spectra of (a) Al-MnO_2 and (b) MnO_2.

Calculation of conduction band and valance band:

As shown in Figure S5, Al-MnO_2 and MnO_2 have valance bands of 1.40 and 1.35 eV. The corresponding standard hydrogen electrode ($E_{VB,\ NHE}$) can be calculated by the formula of $E_{VB,\ NHE}=\varphi + E_{VB} - 4.44$, where φ is the instrument work function (5.0 eV), and the $E_{VB,\ NHE}$ of Al-MnO_2, and MnO_2 are 1.96 and 1.91 eV, respectively.

$$E_{VB} = E_{CB} + E_g$$

As shown in Figure S4, the bandgap (E_g) values of Al-MnO_2 and MnO_2 are 1.40 and 1.90 eV, respectively. Therefore, the E_{CB} of Al-MnO_2 and MnO_2 are 0.56 eV and 0.01 eV, respectively.

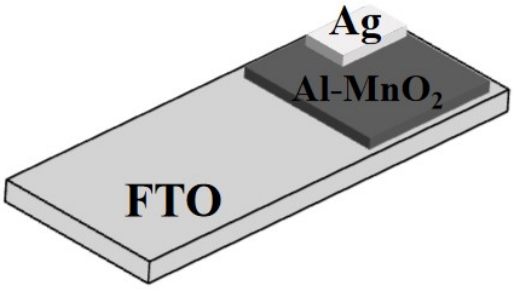

Fig. S6 The model diagram of the FTO/Al-MnO_2/Ag photodetector.

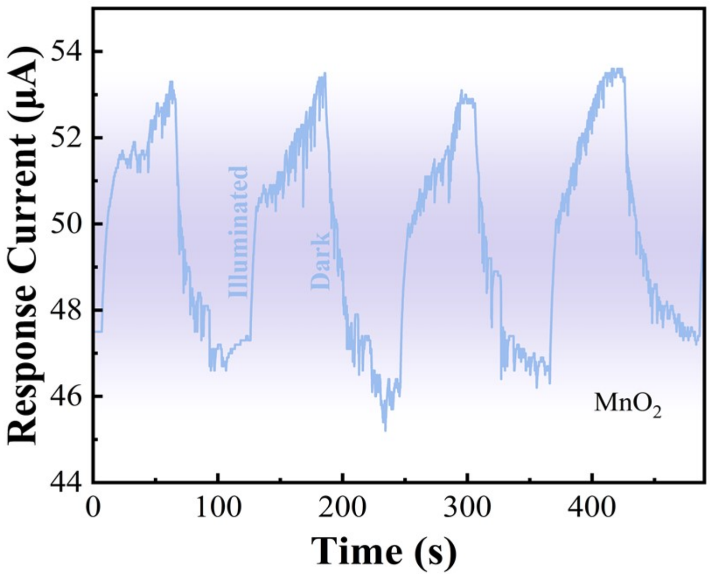

Fig. S7 *I-t* curves of the MnO_2-PD at 0.1 V bias.

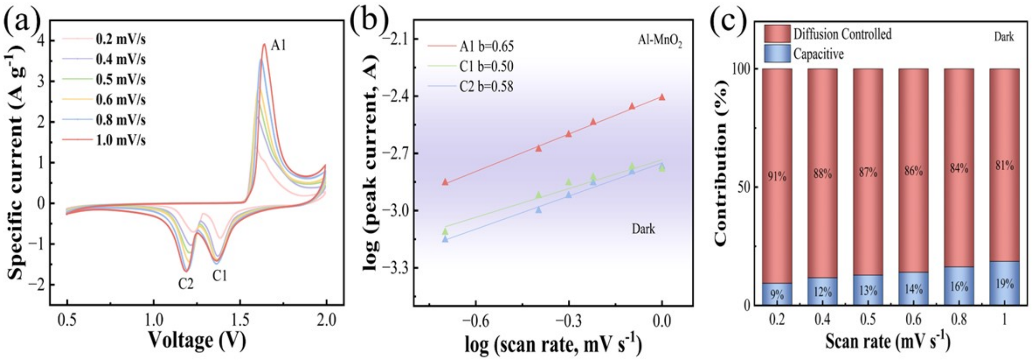

Fig. S8 (a) CV curves of Al-MnO$_2$ under dark. (b) The plot of log (peak current) versus log (scan rate) at each peak on the CV curves under dark. (c) Capacitance contribution and diffusion contribution at different scanning rates under dark.

The charge storage contributions can be split into capacitive-controlled (k_1v) and diffusion-controlled ($k_2v^{1/2}$) parts as a function of the voltage and can be expressed by

$$i(V)= k_1v + k_2v^{1/2} \text{ or } i(V)v^{-1/2}=k_1v^{1/2}+k_2$$

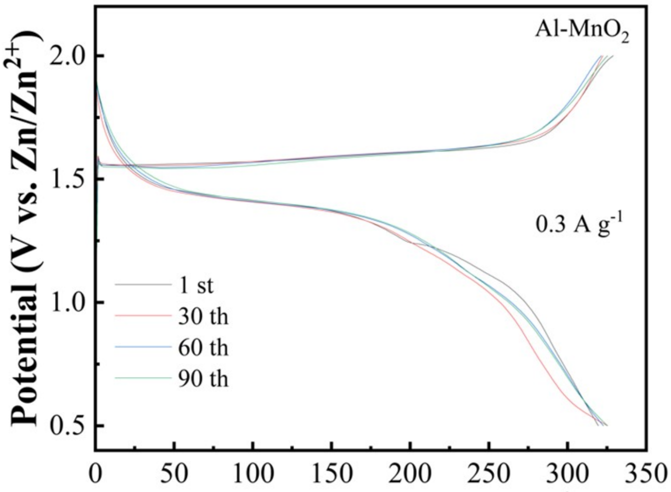

Fig. S9 GCD curve at 0.3 A g^{-1} of Al-MnO$_2$ photocathode under illumination conditions.

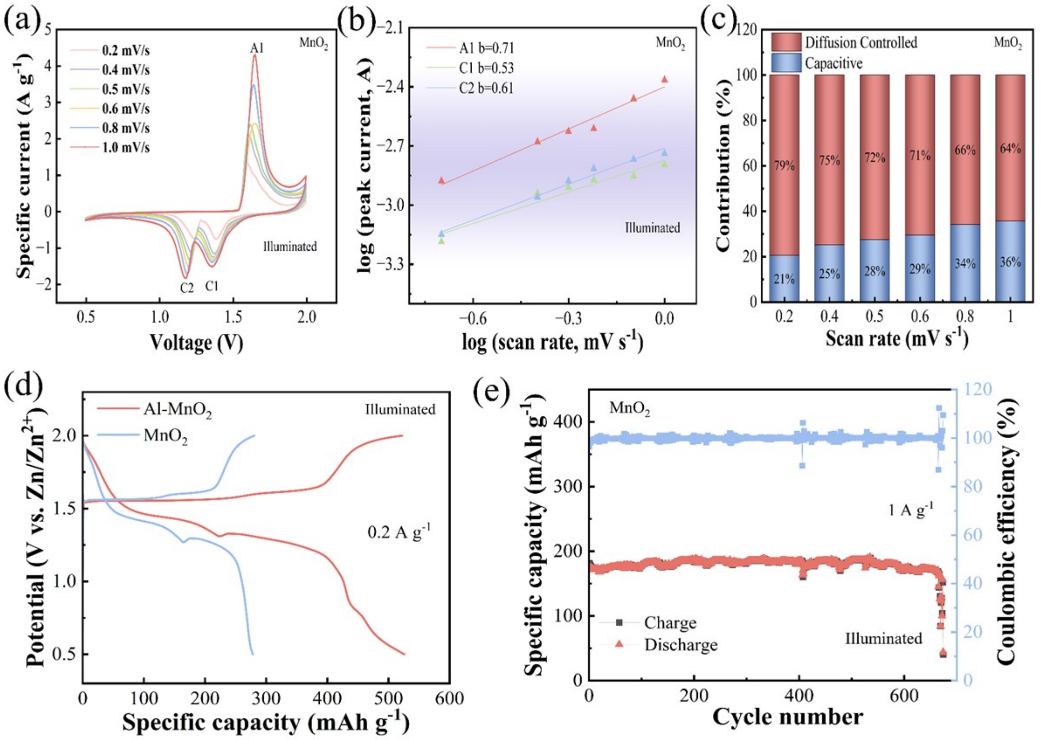

Fig. S10 Electrochemical measurement of MnO_2. (a) CV curves of MnO_2 under light. (b) The plot of log (peak current) versus log (scan rate) at each peak on the CV curves of MnO_2. (c) Capacitance contribution and diffusion contribution at different scanning rates under illumination of MnO_2. (d) GCD curve at 0.2 A g^{-1} under light conditions of MnO_2 and Al-MnO_2. (e) The long-term cycling performance at 1 A g^{-1} under illumination conditions of MnO_2.

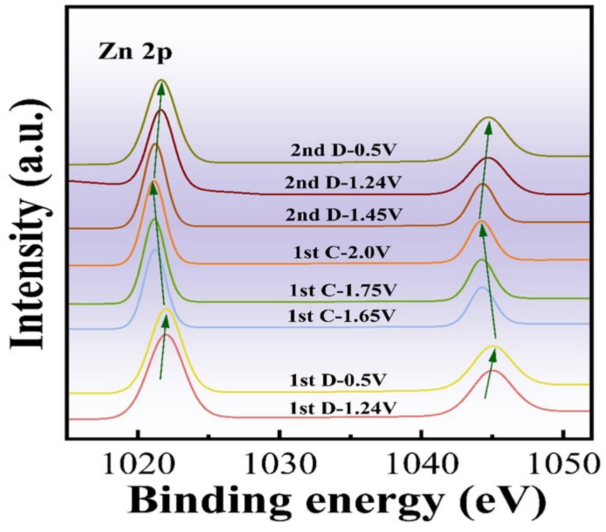

Fig. S11 Zn 2p XPS spectra under illumination.

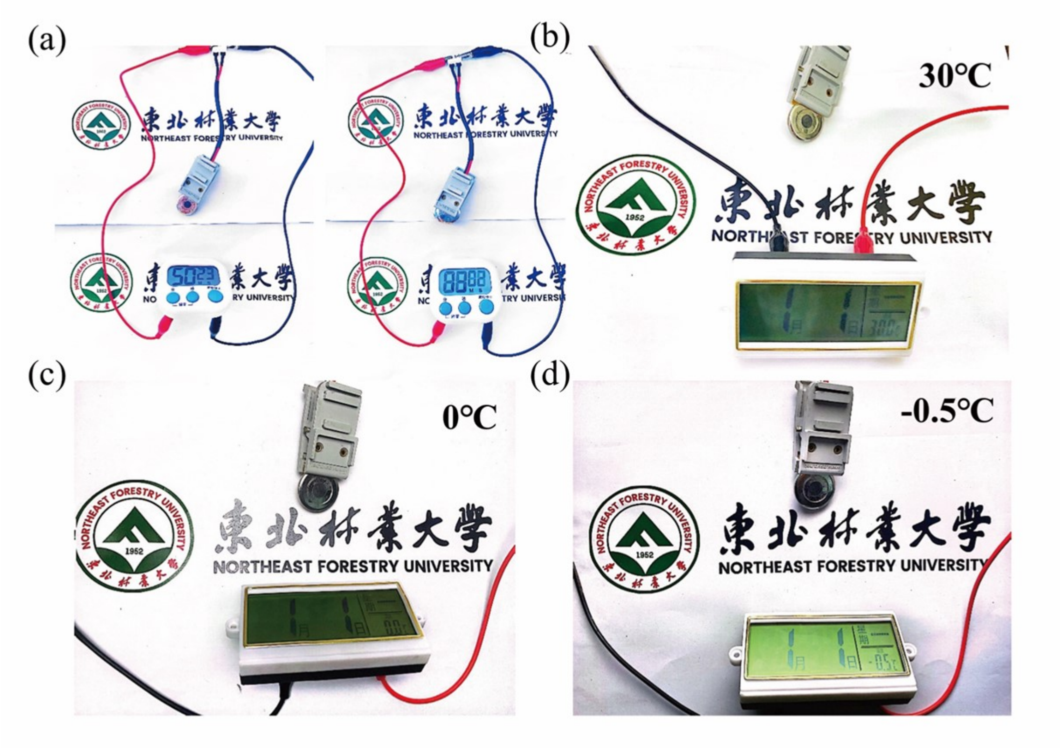

Fig. S12 The practical application of Al-MnO_2-based PAZIB. (a) Al-MnO_2-based PAZIB applies to an electronic timer under light and dark. (b-d) Al-MnO_2-based PAZIB applies to an electronic calendar at different temperatures.

Table S3. The comparison of different photocathodes for PAZIB.

Electrode material	Specific capacity (Illuminated）	capacity retention（Illuminated)	Reference
VO_2-rGO	315 mAh g^{-1} at 200 mA g^{-1}	79% over 250 cycles (5 A g^{-1}, λ≈455 nm)	1
V_2O_3@CSs	463 mAh·g^{-1}at 0.5 A·g^{-1}	61% over 3000 cycles (10 A g^{-1}, λ≈550 nm)	2
TiO_2/BT/Cl-GQDs/MoO_3-NRs	240 mAh g^{-1} at 21 mA g^{-1}	94.7% over 200 cycles （21 mA g^{-1}, 1 sun）	3
MoS_2/ZnO	340 mAh g^{-1} at 100 mA g^{-1}	69% over 200 cycles (500 mA g^{-1}, λ≈455 nm)	4
C@VO_2/ZnO	339.3 mAh g^{-1} at 500 mA g^{-1}	80.98% over 300 cycles （1 A g^{-1}, λ≈365 nm）	5
MoS_2/C	355 mAh g^{-1} at 100 mA g^{-1}	74% over 200 cycles (500 mA g^{-1}, 1 sun)	6
SnO_2@MnO_2	598 mAh g^{-1} at 100 mA g^{-1}	90% over 500 cycles (1 A g^{-1}, 1 sun)	7
ZnO-VO_2	432mAh g^{-1} at 200 mA g^{-1}	/	8
$MoSe_2$-V_{Se}	234.7 mAh g^{-1} at 100 mA g^{-1}	/	9
V_2O_5-P3HT- rGO	370 mAh g^{-1} at 50 mA g^{-1}	/	10
MoS_2/SnO_2 QDs@CC	366/320 mAh g^{-1} at 100 mA g^{-1}	/	11
Al-MnO_2	526 mAh g^{-1} at 200 mA g^{-1}	96% over 1000 cycles （1 A g^{-1}, 1 sun）	Our work

References

1. B. Deka Boruah, A. Mathieson, S. K. Park, X. Zhang, B. Wen, L. Tan, A. Boies and M. De Volder, *Adv. Energy Mater.*, 2021, **11**, 2100115.
2. Y. Zhao, T. He, J. Li, C. Zhu, Y. Tan, K. Zhu, S. Chou and Y. Chen, *Angew. Chem. Int. Ed.*, 2024, **63**, e202408218.
3. B. Kaur, D. Maity, P. Y. Naidu and M. Deepa, *Chem. Eng. J.*, 2023, **468**, 143835.
4. B. D. Boruah, B. Wen and M. De Volder, *ACS Nano*, 2021, **15**, 16616-16624.
5. Z. Ding, T. Jiang, W. Zhao, Z. Luo, H. San, S. Li, X. Li and L. Zhang, *Energy Storage Mater.*, 2024, **71**, 103646.
6. M. Cao, D. Wang, Y. Feng, X. Gu and J. Yao, *J. Mater. Chem. A*, 2024, **12**, 5924-5930.
7. X. Gao, D. Tian, Z. Shi, N. Zhang, R. Sun, J. Liu, H. S. Tsai, X. Xiang and W. Feng, *Small*, 2024, **20**, 2405627.
8. B. Deka Boruah and M. De Volder, *J. Mater. Chem. A*, 2021, **9**, 23199-23205.
9. X. Chen, A. Zhang, H. Zou, L. Li, Q. Zhu and W. Zhang, *Energy Storage Mater.*, 2024, **70**, 103457.
10. B. D. Boruah, A. Mathieson, B. Wen, S. Feldmann, W. M. Dose and M. De Volder, *Energy Environ. Sci.*, 2020, **13**, 2414-2421.

11. X. Wen, Y. Zhong, S. Chen, Z. Yang, P. Dong, Y. Wang, L. Zhang, Z. Wang, Y. Jiang, G. Zhou, J. Liu and J. Gao, *Adv. Sci.*, 2024, **11**, 2309555**.**